Analysis of Compressed Sensing Based CT Reconstruction with Low Radiation

Wen Hou
Faculty of Science, Engineering and Technology
Swinburne University of Technology, Vic 3122, Australia
Email: wenhou@swin.edu.au

Cishen Zhang
Faculty of Science, Engineering and Technology
Swinburne University of Technology, Vic 3122, Australia
Email: cishenzhang@swin.edu.au

***Abstract*—The property of the system matrix of fan-beam computed tomography (CT) is investigated to achieve low radiation dose while reserve good reconstruction quality through compressed sensing (CS). To reduce the radiation dose, scanning data is under-sampled in both the view and bin direction. For limited-angle scanning, two sampling patterns are adopted: golden-angle and random-angle. For sparse bin setting, the reduced detectors are either evenly or randomly distributed. The analysis is conducted based on point spread function (PSF) and Fourier slice theorem (FST), respectively. The simulation results verify the correctness of the analysis and it is shown that low radiation CT reconstruction can be achieved with random detectors and golden-angle scanning.**

***Keywords*—Computed tomography; Compressed sensing; Medical imaging; Point spread function; Fourier slice theorem**

I. Introduction

The significant clinical benefits of computed tomography (CT) in health care were immediately recognized following its introduction into clinical practice in 1972, when Sir Godfrey Hounseld at EMI patented the first CT scanner. Since it was born, this imaging technology has an extensive growth in the number of CT scanners and frequency of CT examinations. Globally, CT scanning has a contribution of over 44% to the total collective effective dose equivalent from medical exposures. The credit of its popularity goes to its capability of providing a wide coverage of the area of interest in a short time, high spatial resolution and ease of operation. Hence, as a popular and useful medical tool, CT plays an important role in the diagnosis and thus benefits patients greatly. In general, the image quality of CT is proportional to the radiation dose. On the other hand, it is known that x-ray radiation leads to ionization of body cells and increased radiation dose raises the risk of cancer. Thus to reduce the x-ray radiation dose to patients and in the mean time preserve the imaging quality has been a significant and challenging problem in CT development.

The conventional CT acquires projection data over a number of view angles and uses filtered back-projection (FBP) [1] method for reconstruction. The number of x-ray projections and data acquisitions for satisfactory image reconstruction is determined by the well known Shannon-Nyquist sampling theorem. Recently, iterative reconstruction techniques (IRT) [2]–[4] has been shown to be capable of reconstructing the image using far few data samples. Specifically, the compressed sensing (CS) technology [5]–[11] has been demonstrated to be a powerful technology for recovering signals from incomplete measurements through optimization methods and been applied to many applications. There have been a number of CS based techniques applied to CT reconstruction problems subject to under-sampled or noisy data [12]–[15]. The key ideas are that CT images can be sparsely represented by some linear transformation and penalizing the norm of the image in the sparsified domain can enable recovery of the unknown image from highly under-sampled data. The application of CS brings great benefits of radiation reduction. It hence has become one of the central topics in medical imaging [16], [17].

The existing works on CT and CS can be roughly divided to two classes. One class is devoted to the reconstruction accuracy through different optimization conditions and algorithms [16]–[20], the other is devoted to the reconstruction speed and the data storage [15], [21], [22] as CT, especially 3D CT, requires a large system matrix. What is seldom discussed, as mentioned in [23], is that the theoretical results from CS do not extend to the CT setting. There is a fundamental lack of understanding about which type of under-sampling is favorable for post CS reconstruction. The reason is that CS requires the sampling matrix in the sparsifying domain to meet the restricted isometry property (RIP), which can't be tested by any known polynomial-time algorithm. In other words, it is the key challenge to achieve incoherence in designing CT data acquisition methods for the successful CS reconstruction. Paper [23] develops quantitative notions for under-sampling based on the condition number of the system matrix, which just addresses invertibility and stability. Paper [24] uses the maximum of the sidelobe-to-peak ratio of point spread function (PSF) to measure the incoherence. In this paper, we select the system matrix class for a 2D circular fan-beam geometry using a square-pixel array and investigate the property of the under-sampled system matrix in light of RIP with two tools: PSF and Fourier slice theorem (FST). The main contribution of this paper is to provide understanding of CS based CT image reconstruction and guideline for the design of low radiation CT scan and reconstruction.

The rest of paper is organized as follows. Section II gives introduction of fan-beam CT data acquisition, CS formulation, and the CS based regularized optimization algorithm for CT reconstruction. Different sampling schemes and the analysis of their impacts on reconstruction are presented in Section III. In Section IV, the experimental results show consistency with the theoretical analysis and the index proposed is more sensitive than the one in [24]. Conclusions are drawn in Section V.

978-1-4799-6120-7/14/$31.00 ©2014 IEEE

II. BACKGROUND

A. Fan-beam computed tomography

The main part of a typical CT scanner is a doughnut shaped gantry that consists of a set of X-ray sources and detectors on opposite sides. The sources emit X-rays that are attenuated when passing through the object and then detected at the detectors, from which an intensity map of the transmission coefficients at various points in the object can be reconstructed. There are different configurations of the X-ray sources and detectors, from the early generation of parallel-beam scan to the currently popular cone-beam spiral scan. In this work, we will take fan-beam projections for simplicity and the results can be extended to other configurations. The basic configuration of fan-beam CT is as follows: a point source of radiation emanates a fan-shaped beam, and on the other side of the object a bank of detectors acquires all the measurements in one fan simultaneously. The source and the entire bank of detectors are rotated to generate the desired number of fan projections. The data acquisition geometry [25] is illustrated in Fig. 1. It shows that the X-ray source travels along a circular trajectory, denoted by $\underline{a}(\lambda) = (R\cos\lambda, R\sin\lambda)^T$, where $\lambda \in [0, 2\pi)$ is the rotation angle, R is the distance between the source and the rotation axis, and the superscript T stands for the transpose operator. The curved detector array lies on a circle of radius D centered at the source. Any ray in the fan beam is specified by an angle $\gamma \in [-\gamma_m, \gamma_m]$ that increases in the clockwise direction. The definition of γ_m is as follows. Assume the object is compactly supported in a centered circular field of view (FOV), the value of $|\gamma|$ for each of the two rays tangent to the FOV is denoted by γ_m.

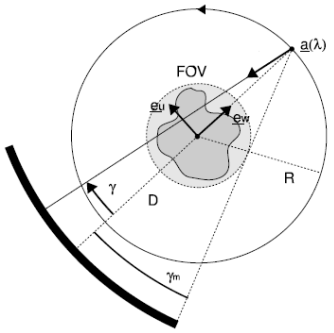

Fig. 1. Fan-beam acquisition geometry with a curved detector

B. Compressed sensing

Compressed sensing [26] is an emerging technology which can achieve perfect signal recovery from much fewer measurements than usually required by Shannon-Nyquist criterion. It exploits the sparseness or compressibility of signals in a predefined basis/frame and its required number of measurements is proportional to the number of non-zero elements in the sparse representation of signals [27].

In what follows, $\mathbb{C}$ denotes the set of complex numbers. I is the identity matrix. $||\cdot||_p$ is the p-norm operator. For a vector object $x \in \mathbb{C}^N$:

$$\begin{aligned} ||x||_p &:= (\sum_{\ell=1}^{N} |x_\ell|^p)^{1/p}, 1 \le p < \infty \\ ||x||_0 &:= |\text{supp} \quad x| \end{aligned}$$

where supp x denotes the support of x. x is s-sparse if $|\text{supp} \quad x| \le s$.

For a matrix $A = (a_{jk}) \in \mathbb{C}^{K\times N}$, the ℓ_2 norm and Frobenius norm is defined as:

$$\begin{aligned} ||A||_2 &= \sigma_{\max}(A) \\ ||A||_F &= \sqrt{\sum_j \sum_k |a_{jk}|^2} \end{aligned}$$

where $\sigma_{\max}(A)$ denotes the largest singular value of A. Besides, it is known that

$$||A||_2 \le ||A||_F$$

CS assumes a linear measurement model, in which a small number of linear measurements $b \in \mathbb{C}^K$ of some unknown quantity of interest $x \in \mathbb{C}^N$ are acquired according to:

$$b = Ax \tag{1}$$

where $A \in \mathbb{C}^{K\times N}$stands for the sampling matrix with $K \ll N$. The reconstruction can be achieved by solving the well-known basis pursuit problem:

$$min \quad ||x||_1 \quad s.t. \quad Ax = b \tag{2}$$

The CS theory requires that the matrix A satisfies the restricted isometry property (RIP). Define the isometry constant δ_s of a matrix A as the smallest number such that

$$(1-\delta_s)||x||_2^2 \le ||Ax||_2^2 \le (1+\delta_s)||x||_2^2 \tag{3}$$

holds for all s-sparse vectors. RIP claims that if $\delta_{2s} \le \sqrt{2}-1$, we can find a unique s-sparse solution for $b = Ax$. There is currently no known polynomial-time algorithm to test whether a given matrix satisfies the RIP.

C. Regularized optimization for CS_CT reconstruction

The CS based CT reconstruction problem can be formulated as:

$$min \quad ||\psi x||_1 \quad s.t. \quad Ax = b \tag{4}$$

where ψ is the sparsifying transform, x is the column-wise vector of the object, b is the projection vector and A is the system matrix based on linear intersection model. When the observation is noisy, the object can be reconstructed through:

$$min \quad ||\psi x||_1 + \frac{\epsilon}{2}||Ax-b||_2^2 \tag{5}$$

where $\epsilon > 0$ is the penalty parameter. The first part in the objective function is the regularization term and the second is often referred to as fidelity term to ensure data consistency. ψ is dependent on image property, and currently total variation (TV) regularization [28] is a popular choice. TV regularization would succeed when the gradient of the underlying image is sparse, i.e. the image possesses piecewise constant property.

The TV minimization problem is solved by the algorithm TVAL3 [29], which is favorable in terms of reconstruction quality and speed. With the input of the sampling matrix A and the measurements b, it approximately minimizes the augmented Lagrangian function by an alternating direction scheme and updates multipliers until the reconstruction error is small enough.

III. Low-radiation CT system design

A. Different sampling schemes

For a low-radiation CT system, sparse angle and sparse bin setting are used. The former one can be realized by the fast on-off switching of tube power and the later one requires a multi-slit collimator to be placed in between a tube and a patient [30]. In the sparse angle case, λ is a vector ranged in $[0 \quad 180 + 2\gamma_m]$. The entries come from the golden-angle [31] or the random-angle setting. For golden-angle scanning, radial projections are successively incremented by the golden angle $\frac{\sqrt{5}-1}{2} \cdot 180^o \approx 111.25^o$. The golden-angle scheme can generate the sets of projections with relatively uniform angular spacings, regardless of the number of radial projections in the set. A relatively well-distributed set of 10 projections is shown in Fig. 2(a), where each line connects the x-ray source location and the center of the object. For random-angle scanning, the angle distribution is random and it is shown in Fig. 2(b). In the sparse bin case, the number of rays is much smaller than normal sense for each angle. Two patterns are considered: the detector distribution is either even or random. Note here in random case, the distribution varies at each angle.

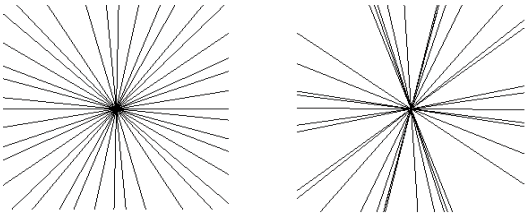

(a) *Golden-angle* (b) *Random-angle*

Fig. 2. Different angle-sampling schemes

B. Index based on PSF

Theorem.

The isometry constant δ_s of $A \in \mathbb{C}^{K\times N}$ with normalized columns possesses the following property [32]:

$$\delta_s = \max_{S\subset[N],|S|\leq s} ||A_S^* A_S - I||_2 \leq ||A^* A - I||_F$$

where $[N] := 1, 2, \cdots, N$ and $|S|$ is the cardinality of S, $A_S = (a_j)_{j\in S}$, i.e. it is the column sub-matrix of A consisting of the columns indexed by S,

Proof.

The definition of the isometry constant is equivalent to

$$|||Ax||_2^2 - ||x||_2^2| \leq \delta_s ||x||_2^2,$$

$$\forall S \subset [N], |S| \leq s, \forall x \in \mathbb{C}^N, \text{supp} \quad x \subset S$$

Left hand side equals $| < (A^*A - I)x, x > |$. Taking the supremum over all $x \in T_s = \{x \in \mathbb{C}^N, ||x||_2 = 1, ||x||_0 \leq s\}$ shows:

$$\begin{aligned} \delta_s &= \sup_{X\in T_s} | < (A^*A - I)x, x > | \\ &= \max_{S\subset[N],|S|\leq s} ||A_S^* A_S - I||_2 \\ &\leq \max_{S\subset[N],|S|\leq s} ||A_S^* A_S - I||_F \\ &\leq ||A^* A - I||_F \end{aligned}$$

According to the theorem, instead of calculating the isometry constant directly, we can measure the Frobenius norm of $A^*A - I$. A^*A is recognized as the point spread function (PSF) in Donoho's work [33], [34]:

$$\text{PSF}(i; j) = e_j^* A^* A e_i, \tag{6}$$

where e_i and e_j is the ith and jth vector of natural basis, respectively. PSF is a natural tool for measuring incoherence. It measures the contribution of a unit-intensity pixel at the ith position to a pixel at the jth position. With Nyquist sampling there is no interference between pixels and $\text{PSF}(i; j)_{i\neq j} = 0$. Under-sampling causes pixels to interfere and assigns nonzero values to $\text{PSF}(i; j)_{i\neq j}$. A nonzero value of PSF at $(i; j)$ means that linear reconstruction of pixel i suffers interference by a unit impulse at pixel $j \neq i$. Since CS requires the aliasing artifacts due to under-sampling to be incoherent, we expect $\text{PSF}(i; j)_{i\neq j}$ to be noise like. From energy view, the PSF measures the tendency of zero-filled linear reconstruction to leak energy from the true underlying source pixel to other pixels. This energy is shown as blurring or aliasing artifacts in the reconstructed image. In designing the sampling matrix, such energy leakage is expected to spread quasi-uniformly across the image.

To determine the impacts of sampling schemes on reconstruction quality, the Frobenius norm of $A^*A - I$, recorded as Υ , is adopted as the quantified index. It is shown as follows in terms of PSF with normalized-column A:

$$\Upsilon \quad = \quad ||\text{PSF} - I||_F \tag{7}$$

Satisfactory reconstruction can be expected when Υ is small.

C. Analysis based on FST

FST claims that in parallel-beam CT, the 1D Fourier transform of the projections is equal to the 2D Fourier transform of the image evaluated on the line that the projection was taken on. That the RIP of Fourier transform matrix is well defined inspires us to analyze the sparse sampling effect via decomposing the system matrix based on FST. We will start with parallel-beam CT, of which the projection line is with the angular and radial coordinates: θ and r.

In what follows, $F_1, F_1^{-1}, F_2, F_2^{-1}$ stand for the 1D and 2D Fourier transform matrix and their inverse, respectively. M and m denote the sufficient and insufficient angle number. $b_{\theta_1}, b_{\theta_2}, \cdots, b_{\theta_m}$ denote the full sinogram at each angle, $B_{\theta_1}, B_{\theta_2}, \cdots, B_{\theta_m}$ are their corresponding 1D Fourier transform, and $pb_{\theta_1}, pb_{\theta_2}, \cdots, pb_{\theta_M}$ stand for the under-sampled sinogram at each angle. I_1 is under-sampling matrix in angle sampling, and $I_{r_1}, I_{r_2}, \cdots, I_{r_M}$ are the ones in detector sampling.

For angle sampling only,

$$Ax = b$$

$$\begin{bmatrix} F_1^{-1} & & & \\ & F_1^{-1} & & \\ & & \ddots & \\ & & & F_1^{-1} \end{bmatrix} I_1 F_2 x = \begin{bmatrix} b_{\theta_1} \\ b_{\theta_2} \\ \vdots \\ b_{\theta_m} \end{bmatrix}$$

$$I_1 F_2 x = \begin{bmatrix} F_1 & & & \\ & F_1 & & \\ & & \ddots & \\ & & & F_1 \end{bmatrix} \begin{bmatrix} b_{\theta_1} \\ b_{\theta_2} \\ \vdots \\ b_{\theta_m} \end{bmatrix}$$

$$I_1 F_2 x = \begin{bmatrix} B_{\theta_1} \\ B_{\theta_2} \\ \vdots \\ B_{\theta_m} \end{bmatrix}$$

Here I_1 is the under-sampling matrix, choosing the 2D Fourier coefficients at $[\theta_1, \theta_2, \cdots, \theta_m]$. The pattern is as in Fig. 2. Hence, the angle sampling of CT is converted to different star shapes in 2D Fourier domain. Empirically for low-frequency image, more center concentrated sampling pattern outperforms others, which means the regular star is expected to behave better than random star.

For detector sampling only,

$$Ax = b$$

$$\begin{bmatrix} I_{r_1} F_1^{-1} & & & \\ & I_{r_2} F_1^{-1} & & \\ & & \ddots & \\ & & & I_{r_M} F_1^{-1} \end{bmatrix} I_1 F_2 x = \begin{bmatrix} pb_{\theta_1} \\ pb_{\theta_2} \\ \vdots \\ pb_{\theta_M} \end{bmatrix}$$

It can be seen as 2 steps:

Step 1:

$$\begin{bmatrix} I_{r_1} F_1^{-1} & & & \\ & I_{r_2} F_1^{-1} & & \\ & & \ddots & \\ & & & I_{r_M} F_1^{-1} \end{bmatrix} X = \begin{bmatrix} pb_{\theta_1} \\ pb_{\theta_2} \\ \vdots \\ pb_{\theta_M} \end{bmatrix}$$

Step 2:

$$I_1 F_2 x = X$$

Both steps are standard CS problems. In Step 2, I_1 is a fixed-star shape with M lines. To get good results, RIP requires $I_{r_1}, I_{r_2}, \cdots, I_{r_M}$ to choose random samples at each angle.

The relation between the independent variables of the fan-beam projections and parallel projections is

$$r = D \sin\gamma \quad \text{and} \quad \theta = \lambda + \gamma,$$

and shown in Fig. 3. For detector sampling, the distribution conforms to each other in parallel-beam CT and fan-beam CT. It is a little bit more complicated when it comes to angle sampling. Because the ray increment is much smaller than the scanning angle increment, at a fix scanning angle λ, a small cluster of parallel projections can be approximated. Hence, the down-sampling of λ corresponds to the cluster r sampling in parallel-beam CT. The distribution of the clusters are decided

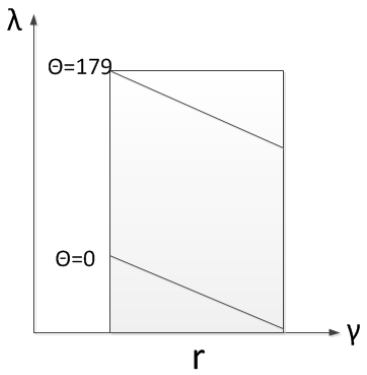

Fig. 3. Relationship between fan and parallel projections

by the pattern of λ, which can either be regular or random. Empirically regular cluster sampling of Fourier coefficients does a better job. Hence, the fan-beam CT with golden-angle scanning and random detectors is expected to gain satisfactory reconstructions.

IV. Simulation results

The experimental setting is as follows: The image size is set to be 128×128. The distance from the source to the center of the domain is $R = 2n$. The span of the rays is defined such that from $(2n, 0)$ the first ray hits the point $(n/2, n/2)$ and the last ray hits $(n/2, -n/2)$. We take the reference point of full sampling as in Paper [23] that for a $n \times n$ object, the full sampling comes with $2n$ samples in both the view and bin direction, i.e. $N_{\text{views}} = N_{\text{bins}} = 2n$. To assess the performance of the reconstructions from different sampling patterns, the normalized mean square error (nMSE) is adopted to indicate the closeness between the original image x_0 and the recovered image x:

$$\text{nMSE} = \mathbb{E}\left\{ \frac{||x - x_0||_2}{||x_0||_2} \right\}$$

Two groups of simulations are designed to test the detector and scan angle sampling, respectively. For the first group, fix the view number to be 256. The detector sampling ratio varies from $30\% - 80\%$, with regular and random distribution. For the second group, fix the detector number to be 256. The angle sampling ratio varies from $10\% - 60\%$, with golden-angle and random-angle pattern. Two classes of images are involved as the object, artificial phantom images and real CT images. 20 images are taken from each of class, and nMSE is the mean value. In random sampling case, the values are averaged over 10 groups of experiments as well. The results are recorded in Tab. I and Tab. II, respectively, where μ is the index developed in [24], nMSE1 is for phantom images and nMSE2 for CT images. Two images are picked for visualization in Fig. 4 and Fig. 5.

According to Tab. I and Tab. II , golden-angle and random-bin obtains lower Υ and μ than random-angle and even-bin in under-sampled case, respectively, indicating higher incoherence of the system matrix and better reconstruction through CS. The results of nMSE and visual effects of the images are consistent with the indicator results. It can also be seen from Tab. I and Tab. II that the index developed in this paper is

TABLE I. GROUP1 THE DETECTOR SETTING

	regular detector				random detector			
sampling ratio	$\Upsilon(10^2)$	$\mu(10^{-1})$	nMSE1	nMSE2	$\Upsilon(10^2)$	$\mu(10^{-1})$	nMSE1	nMSE2
30%	2.68	7.65	0.91%	6.65%	2.57	5.84	0.13%	0.65%
40%	2.55	6.78	0.13%	1.96%	2.50	5.63	0.13%	0.23%
50%	2.45	6.78	0.12%	0.61%	2.44	5.53	0.12%	0.18%
60%	2.44	6.15	0.11%	0.23%	2.42	5.50	0.11%	0.16%
70%	2.41	5.70	0.11%	0.16%	2.39	5.37	0.10%	0.15%
80%	2.38	5.40	0.11%	0.15%	2.37	5.29	0.10%	0.14%

TABLE II. GROUP2 THE ANGLE SETTING

	golden angle				random angle			
sampling ratio	$\Upsilon(10^2)$	$\mu(10^{-1})$	nMSE1	nMSE2	$\Upsilon(10^2)$	$\mu(10^{-1})$	nMSE1	nMSE2
10%	3.05	5.67	0.49%	22.75%	3.27	6.08	9.16%	25.87%
20%	2.61	5.35	0.12%	6.96%	2.81	5.62	0.38%	10.78%
30%	2.48	5.37	0.11%	0.95%	2.61	5.42	0.13%	3.41%
40%	2.42	5.34	0.10%	0.28%	2.53	5.45	0.12%	1.00%
50%	2.39	5.31	0.10%	0.19%	2.47	5.38	0.12%	0.61%
60%	2.38	5.29	0.09%	0.16%	2.45	5.35	0.11%	0.28%

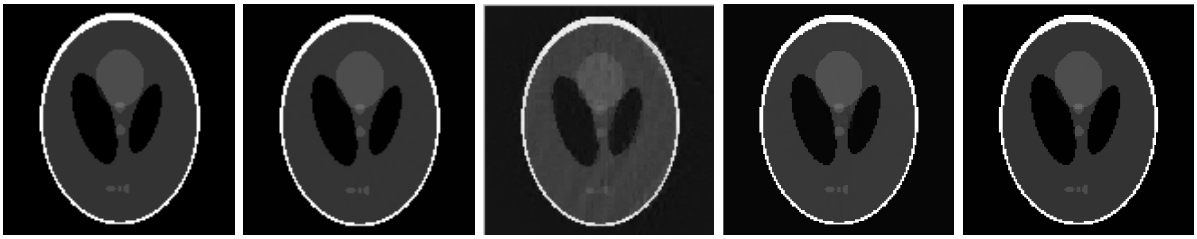

(a) *original image* (b) *golden angle* (c) *random angle* (d) *regular detector* (e) *random detector*

Fig. 4. phantom reconstruction from 10% angle and 30% detector

(a) *original image* (b) *golden angle* (c) *random angle* (d) *regular detector* (e) *random detector*

Fig. 5. CT reconstruction from 30% angle and 30% detector

more sensitive than the one in [24] because Υ is monotonically decreasing with the increase of the sampling ratio while μ shows some exceptions.

V. CONCLUSION

In this paper, the property of the system matrix for fan-beam CT is investigated in the purpose of both reducing the radiation dose and reserving high-quality recovery. With the under-sampled projections, CS is employed for the recovery. Four under-sampling patterns are considered: golden-angle, random-angle, even-bin and random-bin. Two tools are used for the analysis of the impacts of different sampling schemes on reconstructions, PSF and FST. Based on PSF, an evaluation index is proposed: the Frobenius norm Υ of the difference matrix between PSF and the identity matrix. The lower Υ, the better the reconstruction. On the contrary, high off-diagonal interference in PSF implies low-quality recovery. Based on FST, the system matrix is decomposed to Fourier matrix and our aim is converted to the study of sampling on Fourier matrix. It is shown that golden-angle system obtains lower Υ than random-angle and random-bin setting obtains lower Υ than even-bin. Experiments are conducted on phantom image and real CT images, of which the results are measured by normalized mean square error (nMSE). It is consistent with the indicator results, where golden-angle scanning and random-bin setting obtains lower nMSE than the other two, respectively.

With both the theoretical and experimental analysis, the purpose of reducing radiation dose without compromising the reconstruction quality is achieved. The conclusion is drawn that the golden-angle scanning and random bin is most favorable for the post CS based reconstruction.

REFERENCES

[1] A. Ziegler, T. Kohler, and R. Proksa, "Noise and resolution in images reconstructed with FBP and OSC algorithms for CT," *Medical Physics*, vol. 35, pp. 585–598, 2008.

[2] X. L. Xu, J. S. Liow, and S. C. Strother, "Iterative algebraic reconstruction algorithms for emission computed tomography: A unified framework and its application to positron emission tomography," *Medical Physics*, vol. 20, pp. 1675–1684, 1993.

[3] J. Sunnegardh and P. E. Danielsson, "Regularized iterative weighted filtered backprojection for helical cone-beam CT," *Medical Physics*, vol. 35, pp. 4173–4185, 2008.

[4] A. Ziegler, T. Nielsen, and M. Grass, "Iterative reconstruction of a region of interest for transmission tomography," *Medical Physics*, vol. 35, pp. 1317–1327, 2008.

[5] E. J. Candes and J. Romberg, "Quantitative robust uncertainty principles and optimally sparse decompositions," *Foundations of Computational Mathematics*, vol. 6, pp. 227–254, 2006.

[6] E. J. Candes, J. Romberg, and T. Tao, "Robust uncertainty principles: Exact signal reconstruction from highly incomplete frequency information," *IEEE Transactions on Information Theory*, vol. 52, pp. 489–509, 2006.

[7] E. J. Candes and J. Romberg, "Near-optimal signal recovery from random projections: Universal encoding strategies?" *IEEE Transactions on Information Theory*, vol. 52, pp. 5406–5425, 2006.

[8] Y. Tsaig and D. L. Donoho, "Extensions of compressed sensing," *Signal Processing*, vol. 86, pp. 549 – 571, 2006.

[9] D. L. Donoho, "Compressed sensing," *IEEE Transactions on Information Theory*, vol. 52, pp. 1289–1306, 2006.

[10] D. L. Donoho and J. Tanner, "Neighborliness of randomly projected simplices in high dimensions," in *Proceedings of the National Academy of Sciences of the United States of America*, vol. 102, 2005, pp. 9452–9457.

[11] M. Lustig, D. L. Donoho, J. M. Santos, and J. M. Pauly, "Compressed sensing MRI," *IEEE Signal Processing Magazine*, vol. 6, pp. 72–82, 2008.

[12] E. Y. Sidky, C. M. Kao, and X. C. Pan, "Accurate image reconstruction from few-views and limited-angle data in divergent-beam CT," *J. X-Ray Sci. Technol.*, vol. 15, pp. 119–139, 2006.

[13] E. Y. Sidky and X. C. Pan, "Image reconstruction in circular cone-beam computed tomography by constrained, total-variation minimization," *Phys. Med. Biol.*, vol. 53, pp. 777–807, 2008.

[14] G. H. Chen, J. Tang, and S. H. Leng, "Prior image constrained compressed sensing (PICCS): A method to accurately reconstruct dynamic CT images from highly undersampled projection data sets," *Medical Physics*, vol. 35, pp. 660–673, 2008.

[15] X. Jia, Y. Lou, R. Li, and et al, "GPU-based fast cone beam CT reconstruction from undersampled and noisy projection data via total variation," *Medical Physics*, vol. 37, pp. 1757–1760, 2010b.

[16] X. Han, J. Bian, and D. R. Eaker, "Algorithm-enabled low-dose micro-CT imaging," *IEEE Trans. Medical Imaging*, vol. 30, pp. 606–620, 2011.

[17] X. Jia, B. Dong, Y. Lou, and S. B. Jiang, "GPU-based iterative cone beam CT reconstruction using tight frame regularization," *Physics in Medicine and Biology*, vol. 56, pp. 3787–3807, 2011.

[18] J. Bian, J. Wang, X. Han, E. Y. Sidky, L. Shao, and X. Pan, "Optimization-based image reconstruction from sparse-view data in offset-detector CBCT," *Physics in Medicine and Biology*, vol. 58, pp. 205–230, 2013.

[19] P. T. Lauzier and G. H. Chen, "Characterization of statistical prior image constrained compressed sensing. I. applications to time-resolved contrast-enhanced ct," *Medical Physics*, vol. 39, pp. 5930–5948, 2012.

[20] ——, "Characterization of statistical prior image constrained compressed sensing (PICCS): II. application to dose reduction," *Medical Physics*, vol. 40, p. 021902, 2013.

[21] T. Niu and L. Zhu, "Accelerated barrier optimization compressed sensing (ABOCS) reconstruction for cone-beam CT: Phantom studies," *Medical Physics*, vol. 39, pp. 4588–4598, 2012.

[22] J. C. Park, B. Song, J. S. Kim, S. H. Park, H. K. Kim, Z. Liu, T. S. Suh, and W. Y. Song, "Fast compressed sensing-based CBCT reconstruction using barzilai-borwein formulation for application to on-line IGRT," *Medical Physics*, vol. 39, pp. 1207–1217, 2012.

[23] J. H. Jrgensen, E. Y. Sidky, and X. Pan, "Quantifying admissible undersampling for sparsity-exploiting iterative image reconstruction in x-ray CT," *IEEE Transactions on Medical Imaging*, vol. 32, pp. 460–473, 2013.

[24] M. Lustig, D. Donoho, and J. M. Pauly, "Sparse MRI: The application of compressed sensing for rapid MR imaging," *Magnetic Resonance in Medicine*, vol. 58, pp. 1182–1195, 2007.

[25] F. Dennerlein, F. Noo, J. Hornegger, and G. Lauritsch, "Fan-beam filtered-backprojection reconstruction without backprojection weight," *Physics in Medicine and Biology*, vol. 52, pp. 3227–3240, 2007.

[26] M. Rostami, O. Michailovich, and Z. Wang, "Image deblurring using derivative compressed sensing for optical imaging application," *IEEE Trans. Image Processing*, vol. 21, pp. 3139–3149, 2012.

[27] E. J. Cands and M. B. Wakin, "An introduction to compressive sampling," *IEEE Signal Processing Magazine*, vol. 25, pp. 21–30, 2008.

[28] L. I. Rudin, S. Osher, and E. Fatemi, "Nonlinear total variation noise removal algorithm," *Physica D*, vol. 21, pp. 3139–3149, 1992.

[29] C. Li, "An efficient algorithm for total variation regularization with applications to the single pixel camera and compressive sensing," 2009.

[30] S. Abbas, T. Lee, S. Shin, R. Lee, and S. Cho, "Effects of sparse sampling schemes on image quality in low-dose CT," *Medical Physics*, vol. 40, p. 111915, 2013.

[31] R. W. Chan, E. A. Ramsay, E. Y. Cheung, and D. B. Plewes, "The influence of radial undersampling schemes on compressed sensing reconstruction in breast MRI," *Magnetic Resonance in Medicine*, vol. 67, pp. 363–377, 2012.

[32] H. Rauhut, "Compressive sensing and structured random matrices," *Radon Series Comp. Appl. Math XX*, pp. 1–94, 2011.

[33] D. L. Donoho, Y. Tsaig, I. Drori, and J. L. Starck, "Sparse solution of underdetermined systems of linear equations by stagewise orthogonal matching pursuit," *IEEE Trans. Inform. Theory*, vol. 58, pp. 1094–1121, 2012.

[34] ——, "Image deblurring using derivative compressed sensing for optical imaging application," *IEEE Trans. Image Processing*, vol. 21, pp. 3139–3149, 2012.